electronics

MDPI

Article

Graph-Based Modeling and Optimization of WPT Systems for EVs

Matthew J. Hansen *,†, Greg Droge † and Abhilash Kamineni †

Department of Electrical and Computer Engineering, Utah State University, Logan, UT 84322, USA; greg.droge@usu.edu (G.D.); abhilash.kamineni@usu.edu (A.K.)

* Correspondence: matthew.hansen@usu.edu

† These authors contributed equally to this work.

Abstract: A model of a system of wireless power transfer (WPT) pads is developed, where each WPT pad is modeled as a node and the coupling between pads is modeled as graph edges. This modeling approach is generalized to admit primary, secondary, and booster coils, where power can flow among the pads and a pad can fill multiple roles. An excitation in one pad induces voltage and current in all neighboring pads, causing each pad to act as both a booster coil and either a transmitter or a receiver. Power flow through the entire system can be modeled with the graph structure; the power flow can then be optimized by alternating the phases of the WPT excitations to maximize power transfer. An example is shown where exploiting the graph-based WPT system modeling increases total energy transfer by 25% compared to another method. This increase occurs without altering the geometry of the pads or the magnitude of the pad excitations.

Keywords: wireless power transfer; graphs; optimization; inductive power transfer

check for updates

Citation: Hansen, M.J.; Droge, G.; Kamineni, A. Graph-Based Modeling and Optimization of WPT Systems for EVs. *Electronics* **2024**, *13*, 2154. https://doi.org/10.3390/electronics13112154

Academic Editor: Fabio Corti

Received: 18 April 2024
Revised: 21 May 2024
Accepted: 29 May 2024
Published: 31 May 2024

Copyright: © 2024 by the authors. Licensee MDPI, Basel, Switzerland. This article is an open access article distributed under the terms and conditions of the Creative Commons Attribution (CC BY) license (https://creativecommons.org/licenses/by/4.0/).

1. Introduction

Wireless power transfer (WPT) is becoming increasingly common in various applications, including electric vehicles (EVs). The application of WPT to EVs may alleviate range anxiety [1], reduce battery and EV upfront costs, and preserve battery lifetime. WPT transmits power from a *primary coil*, also called a transmitter or Tx, to a *secondary coil*, also called a receiver or Rx. An excitation, either a voltage source or current source, forces the creation of an electric field (capacitive power transfer, CPT) or a magnetic field (inductive power transfer, IPT) between the primary and secondary; the field draws power from the primary and injects power into the secondary. Emerging WPT applications often employ multiple coils, but the design and control of such applications only consider interactions between two coils. In this work, interactions between all the coils in a system are modeled, and those interactions are exploited to maximize power transfer.

Typically, IPT can achieve greater power transfer over a larger air gap at lower frequency [2], and thus, is more commonly used. Consequently, this work assumes IPT, although the principles could be transferred to a CPT system. For an EV application, the primary and secondary coils are generally poorly coupled; a coupling coefficient of $k = 0.3$ is generally near the upper limit. The coupling coefficient is a value that indicates how much magnetic flux is shared between two coils. By convention, the coupling coefficient varies between 0, indicating no net shared flux, and 1, indicating identical magnetic fields. Sometimes it is also convenient to consider negative coupling factors between 0 and -1 to reflect the reference polarity. The coupling factor is only tangentially related to efficiency; a lower coupling factor requires more inductor current to transmit the same power; while that current can incur resistive losses, the coupling coefficient does not directly correspond to radiative or conductive losses. High power transfer requires a high mutual inductance, which implies very large self-inductances. To counteract some of the reactive power consumed by primary and secondary coils, a WPT circuit usually includes *compensation*,

a capacitive load that supplies reactive power; many different compensation schemes have been developed. The assembly of the coil, compensation, and inverter is sometimes referred to as a *pad*. As WPT pad design [3–5], control [6], and IPT modeling [7,8] are well-studied topics, the questions of dynamic control, compensation, and pad design and not considered herein. Rather, the study investigates the interconnectedness of multiple WPT nodes to optimize power transfer.

The existing literature tends to describe WPT in terms of point-to-point wireless power transfer, with a single primary or a single secondary, rather than as power transfer through an interconnected graph of WPT nodes. Even in DWPT systems that typically include multiple primaries, it is often assumed that primary–primary interactions are negligible and each primary operates more or less independently [9,10]. WPT systems are generally designed to have good primary–secondary coupling, but also generally have *parasitic coupling*; in IPT systems, the parasitic coupling is the mutual inductance that is not designed for power transfer, i.e., primary–primary or secondary–secondary inductance. This parasitic coupling is always present when there are multiple primaries or secondaries, and while it is generally ignored, its effects can be harmful, negligible, or beneficial.

Some emerging WPT applications make use of a WPT network with multiple primaries and secondaries, whether that is to extend the WPT range in dynamic WPT (DWPT), transfer power to various targets, provide three-phase power, or increase the WPT range [4,11–14]. However, none of these works aim to provide a generalized framework for modeling and exploiting parasitic coupling. The work in [11] uses changes in the parasitic primary–primary coupling to detect an approaching vehicle, but power is not transferred along the primary–primary link. In [12,13], multiple primaries and secondaries are considered, but primary–primary coupling and secondary–secondary coupling are not considered. Similarly, the work in [15] presents a harmonics-based scheme to transmit power from a single transmitter to multiple receivers, but the power transmission from the primary to each secondary is designed to be independent. Booster coils, or coils without a conductive connection to an excitation source that are placed between a primary and a secondary coil, are discussed in [14], which increase the distance over which power transfer is achieved. However, there is still a single transmitter coil and a single receiver coil. Other work estimates the existence or position of multiple secondaries, but using parasitic coupling to maximize power transfer is outside the scope of [12,16,17]. The parasitic couplings in a system with either multiple transmitter coils or multiple receiver coils are also considered in [18]; however, that approach only considers either multiple receiver coils or multiple transmitter coils, but not both simultaneously. Moreover, the work in [18] modifies the frequency of the elements, which can limit total power in some cases. Furthermore, it is desired to impose an accurate, optimizable model on an existing system rather than designing a system around the parasitic couplings. The work in [19], although only considering a single WPT pad, bears conceptual and mathematical similarities to the approach developed herein. In [19], current distribution through multiple parallel windings within a single coil is discussed and modeled. Each winding is coupled with the secondary coil, but also with the other, parallel windings; this affects current distribution, losses, and overall primary–secondary coupling. However, multiple primary pads and parasitic coupling are not discussed.

This work aims to exploit parasitic coupling to improve power transfer and present a model that unifies the varying modeling methods for complex WPT systems. This improves the current state of the art in two ways. First, it allows for more accurate modeling of the WPT system, modeling power flow through the network, rather than simply from one primary to one secondary. This results in a unified model that can be used on booster coils, parallel windings, or complex WPT systems with multiple primaries and secondaries. Second, this work also develops a technique to optimize power transfer by altering the phase of each primary in the system. Brief discussions of distributed controllability and multiple-secondary systems are included. To those ends, WPT through a complex system of mutually coupled coils is described with a graph, where each node represents a WPT

unit, and the edges represent mutual coupling. This graph structure allows the practitioner to model and optimize power flow from one point to another throughout the network, rather than through two coupled coils. Multiple applications of this approach exist; the work focuses on an in-motion or dynamic WPT (DWPT) system represented as a series of stationary WPT (SWPT) systems. The system of each SWPT set point can be modeled and optimized with a graph, leading to an optimization of the DWPT system as a whole. This approach yields richer insights than observation at a single set point.

The scope of this paper encompasses the theoretical development and simulation validation of this scheme. The focus of this paper is on the development of this approach, rather than on the integrity of a specific hardware component. Rather, the innovations discussed herein are generally applicable to most WPT systems. Consequently, the experimental validation of this approach and subsequent contributions is deferred for future works.

The paper is organized as follows. Section 2 defines the mathematical background of the system, and describes a method to account for all the paths from one node to another. Section 3 discusses optimal control of a multi-pad system, and addresses some of the capabilities and challenges of this approach. An example of this modeling technique is discussed in Section 4. Section 5 concludes this paper, reiterating key contributions and improvements with this modeling approach.

2. Basic Model

With multiple primaries and secondaries, the interactions become complicated. Once the mathematics of graph-based modeling have been developed; the parasitic couplings can be exploited to increase power transfer. Therefore, it is necessary to mathematically model the parasitic couplings, which is accomplished in this section. In Section 2.1, some notation is defined, followed by a discussion of the complexities of complex WPT systems with three or more WPT pads in Section 2.2. In Section 2.3, a graph is developed to model power flow through complex systems, for which a mathematical model is defined.

2.1. Definition of States

First, note that with any compensation and excitation, a WPT pad can be modeled as either a Norton or Thévenin equivalent circuit; here, it is assumed that the WPT pads are represented as Thévenin circuits, which are excited by a voltage source. Consider a system with Thévenin equivalent circuits on two primary pads and two secondary pads, as seen in Figure 1, where each pad is represented as a graph node. Pad n is excited by a phasor voltage source $\bar{v}_{X,n}$, which drives a current $\bar{i}_n$ through the Thévenin equivalent impedance Z_n and the power transfer coil. The voltage across the Thévenin impedance, $\bar{v}_{Z,n}$ plus the voltage across the coil $\bar{v}_{L,n}$ sums to $\bar{v}_{X,n}$.

Similar quantities can be gathered into a single vector. Assume there are N WPT coils in a system, then define the vectors

$$\begin{aligned} \mathbf{v}_L &= \begin{bmatrix} \bar{v}_{L,1} & \bar{v}_{L,2} & \cdots & \bar{v}_{L,N} \end{bmatrix}^T \\ \mathbf{v}_Z &= \begin{bmatrix} \bar{v}_{Z,1} & \bar{v}_{Z,2} & \cdots & \bar{v}_{Z,N} \end{bmatrix}^T \\ \mathbf{v}_X &= \begin{bmatrix} \bar{v}_{X,1} & \bar{v}_{X,2} & \cdots & \bar{X}_{X,N} \end{bmatrix}^T \\ \mathbf{i} &= \begin{bmatrix} \bar{i}_1 & \bar{i}_2 & \cdots & \bar{i}_N \end{bmatrix}^T \end{aligned} \tag{1}$$

Also, define an *inductance matrix*, noted as L, that collects that self- and mutual-inductance values. The inductance $L_{m,n}$ relates the current through coil m to the voltage induced across coil n. Note that $L_{m,n} = L_{n,m}$.

$$L = \begin{bmatrix} L_{1,1} & L_{1,2} & \cdots & L_{1,N} \\ L_{2,1} & L_{2,2} & \cdots & L_{2,N} \\ \vdots & \vdots & \ddots & \vdots \\ L_{N,1} & L_{N,2} & \cdots & L_{N,N} \end{bmatrix} \tag{2}$$

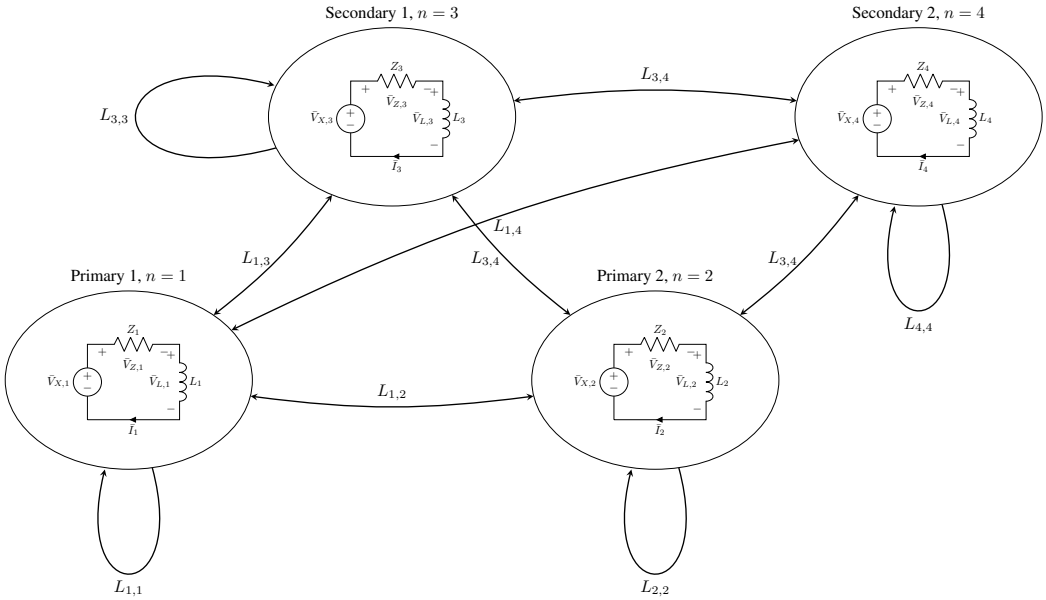


Figure 1. Diagram of WPT system as a graph, with each edge representing an inductance and each oval corresponding to a node in the graph or a WPT pad in the circuit.

The problem can be mapped to a graph, as in Figure 1, which uses the notation defined above. Each node corresponds to a single pad, and the coupling between pads is expressed as an edge. The coupling can be interpreted with magnetic flux, induced voltage, or power flowing along the edges of the graph, with each primary or secondary pad represented with a node. States at each node are the relevant quantities in the pad, i.e., current through the coils and voltages across the inductors, and the input to each node is the excitation voltage.

In Figure 1, there are multiple power transmission paths from primary 1 to secondary 1 and multiple paths from primary 2 to secondary 1. The net effect of all the transmission paths is captured in the equation above. With this formulation, the matrices Z and L are both symmetric, implying that the inverse matrix is also symmetric.

2.2. Difficulties of Complex WPT Systems

Most studies in the literature consider a system with only a single primary pad and a single secondary pad, where the number of WPT pads $N = 2$. In that case, the power flow is straightforward and can be analyzed with tools like the transformer T-model or the reflected impedance.

However, those tools are not appropriate for a more complex network. Consider the WPT system shown in Figure 1, which has two primary pads and two secondary pads. Each coil couples with the others, and the interactions can be difficult to model. For example, suppose primary 1 ($n = 1$) is excited with an excitation voltage $\bar{v}_{X,1}$, which induces currents in all the other pads, which reflect a voltage to $\bar{i}_{L,1}$. However, the current $\bar{i}_2$ also affects the current $\bar{i}_3$, which affects the voltage seen at $\bar{v}_{L,1}$. Because the pads interact with each other through their neighbors, the interactions between a pad and each of its neighbors cannot be analyzed in isolation and the interactions across the system must be analyzed simultaneously.

Some pads may be poorly coupled to others, and the system may be reasonably represented by a partially connected graph, where low-value edges are rounded to 0. In

very complex systems, there may be an improvement in computational load with a partially connected graph, or it might be computationally heavy to generate all the edge weights. However, if all the relevant inductance values are generated by an FEM solver, or if the graph is small, there may not be an appreciable advantage to pruning low-weight edges.

In this paper, the edge weight is the inductance between coils in each node/pad; inductance is defined as the ratio of voltage across a coil to the frequency and current through a coupled coil Each coil is coupled perfectly with itself. When the voltage and current are measured on the same coil, the ratio is self-inductance. Each edge of the graph in Figure 1 corresponds to one or two elements of L; the edges between distinct nodes are represented twice in L, i.e., $L_{m,n}$ and $L_{n,m}$, and the edges leading to and from the same node are represented only once each in L, i.e., $L_{n,n}$. The edges represented twice in L imply that current through coil m induces a voltage on n, and the same current through n induces the same voltage on m.The graph structure is encoded within the symmetric inductance matrix L, and the interactions between states at any node are mediated through an impedance matrix Z.

2.3. Mathematical Model

Consider the WPT system shown in Figure 1, with representative coupling values. This represents a snapshot of a dynamic WPT (DWPT) system, where two secondaries move across two primary pads. Let the switching frequency, or the frequency of the AC voltage excitation, be given as ω, with units of radians per second.

Even in a DWPT scenario, the dynamics are typically dominated by the switching: The voltages across the inductors in a dynamic system are given by

$$\mathbf{v} = L\frac{d\mathbf{i}}{dt} + \frac{dL}{dt}\mathbf{i}. \tag{3}$$

Expressing the voltage and current quantities as phasors, Equation (3) can be expressed as

$$\mathbf{v} = \left(j\omega L + \frac{dL}{dt}\right)\mathbf{i}. \tag{4}$$

Typically, the switching frequency is high relative to the inductance values. A reasonable mutual inductance value in a DWPT system is 5 µH, and pads could be spaced on 1 m intervals. If a vehicle travels at 30 m/s, then

$$\left\|\frac{dL}{dt}\right\| \approx 0.2\,\mu\text{H/s}. \tag{5}$$

However, according to existing standards, a common switching frequency is 85 kHz [20]; assuming the same typical inductance value of 5 µH yields

$$\|j\omega L\| \approx 2\,\text{H/s}. \tag{6}$$

Although very approximate, Equations (5) and (6) show that the dynamics due to switching are roughly six orders of magnitude more important than dynamics due to changing inductances; therefore, Equation (3) can be approximated as

$$\mathbf{v} = L\frac{d\mathbf{i}}{dt} \tag{7}$$

and the DWPT system can be analyzed as a series of stationary WPT systems. For simplicity, only one secondary is considered in this paper, except for the discussion on multiple secondaries in Section 3.3.

The defining equations are the voltage-balancing and the inductance equation. Using the vectors defined in Equation (1), the relevant equations are

$$\begin{aligned} \mathbf{v}_L &= j\omega L\mathbf{i} \\ \mathbf{v}_Z &= Z\mathbf{i} \\ \mathbf{v}_X &= \mathbf{v}_L + \mathbf{v}_Z \end{aligned} \tag{8}$$

The defining equations can be solved for $\mathbf{i}$:

$$\mathbf{i} = (j\omega L + Z)^{-1}\mathbf{v}_X. \tag{9}$$

The expression in Equation (9) shows that $\mathbf{v}_X$ is an input to the system; the excitation voltages can be arbitrarily, independently, and directly selected. The current vector $\mathbf{i}$ represents a state, which cannot be directly set but is a consequence of the inputs. Note that $(j\omega L + Z)$ is assumed to be invertible; this is addressed more fully in Section 3.2. For convenience, define the matrix

$$B = (j\omega L + Z)^{-1} \tag{10}$$

and let $b_{m,n}$ be the element in row m and column n of B.

It is common to model WPT as a series of transmitters or receivers. A transmitter–receiver paradigm can be imposed on the graph-based approach. It may appear simple to calculate the energy transferred from one point to another directly with only the inductance matrix L, but as one pad induces a current in a neighboring pad, the induced current induces more current in its neighboring pads. This is the motivation for the graph-based approach, that multiple transmission paths exist simultaneously. However, Equation (9) allows the system designer to simplify the graph to a series of independent paths, reducing the multiple paths to a single link. Section 3 further develops how the standard transmitter–receiver model of WPT is inherent in the proposed graph-based model.

This approach is general enough to model most linear WPT systems, but the graph underlying this structure is powerful enough to quickly and powerfully model complicated systems, like that discussed in [14]. Even for a system for which this approach may not directly work, simple modifications to the equations presented here may make this approach applicable. One example is the LCC-compensated circuit used in [9,11,21], where the Thévenin equivalent impedances and excitation voltages are all infinite. In such a case, a very similar approach to that taken herein, but using Norton equivalent circuits, could be used to model the system.

3. Control Optimization

Once all the couplings in a system have been modeled, the contributions of each primary pad to the current flowing in the secondary are orthogonalized; the current can be expressed as a weighted sum of the excitation voltages, where the weights can be understood as admittances. This separates the contributions of each voltage excitation, which allows each to be optimized independently. This section describes how that optimization is achieved.

The utility of the WPT graph is highlighted with an optimization of power flow. That is, given a fixed secondary phase, it is desired to control the phase of each primary pad to maximize power transfer. As mentioned earlier, most of this section assumes two primary pads and one secondary pad.

Consider the case where the secondary operates at the reference phase, meaning that the phasor values in the voltage excitation vector $\mathbf{v}_X$ corresponding to the secondary excitations are entirely real. Letting $v_{X,s}$ be the element of $\mathbf{v}_X$ corresponding to the secondary,

$$v_{X,s} \in \mathcal{R} \tag{11}$$

Because all impedances in the system are typically purely reactive, any real excitation voltages induce imaginary currents, and any imaginary excitation voltages correspond to real currents. In a reactive circuit excited by a single source, all the currents with be out of phase from the voltage excitation by 90°. Because the compensation is linear, the currents

induced by each excitation sum. Consequently, the real power absorbed by a secondary is maximized when the current through the secondary excitation is parallel to the secondary excitation voltage, which will occur when the primary excitation voltage is offset from the secondary excitation by 90°. In a general case, the primaries should each operate at ±90° relative to the phase of the secondary, so that the current induced on the secondary voltage source is in phase with that voltage source. However, there remains the question of whether a given primary should lead or lag the secondary; that determination is the focus of this section.

3.1. Omniscient Optimal Control

With an omniscient controller, calculating the optimal control is straightforward. Without loss of generality, let the excitation voltage of the secondary be defined by the real, positive phasor $\bar{v}_{X,s}$, where s is the index of the secondary pad. With the voltages and currents defined as in Figure 1, the complex power supplied by the voltage source is given by

$$\bar{v}_{X,s}\bar{i}_s^*, \tag{12}$$

where $\bar{i}_s^*$ is the complex conjugate of the current $\bar{i}_s$. Here, $\bar{v}_{X,s}$ is a real constant, and the other quantities in $\mathbf{v}_X$ are the variables of optimization. Maximizing the real power transferred is expressed as

$$\max_{\mathbf{v}_X \setminus v_{X,s}} \Re\left(-\bar{i}_s^* \bar{v}_{X,s}\right) \tag{13}$$

Two constraints are necessary. First, it is necessary that the circuit equations encoded in Equation (9) are satisfied, so that the optimization result is realizable. Second, the voltages must be bounded. There are two reasons for the excitation voltages to be bounded. First, the excitation voltages are typically physically bounded by the DC bus voltage (the Thévenin equivalent voltage can be unbounded, but such a case would best be modeled by a Norton equivalent circuit); the voltage applied across the system at any moment may not exceed the DC supply voltage. Second, without a constraint on the norm of the excitation voltages, the optimization would maximize the norms of the voltages, rather than optimizing the phase. An optimizer is unlikely to solve the problem, and no insight into the system is gained by noting that infinite excitation voltages can transfer infinite power. Letting α_n be a real-positive value describing the maximum excitation current for node n in the graph (either a primary or secondary pad), the full optimization can be expressed mathematically as

$$\begin{aligned} &\max_{\mathbf{v}_X} \Re\left(-\bar{i}_s^* \bar{v}_{X,s}\right) \text{ s.t.} \\ &\|\bar{v}_{X,n}\| \leq \alpha_n \forall n \\ &\mathbf{i} = B\mathbf{v}_X. \end{aligned} \tag{14}$$

This optimization is trivial once the inverse matrix B is found. Using the element-wise notation for B, the objective function is expanded to consider each voltage excitation separately:

$$\Re\left(-\bar{i}_s^* \bar{v}_{X,s}\right) = \sum_n \Re\left(-\bar{v}_{X,s} b_{s,n}^* \bar{v}_{X,n}^*\right). \tag{15}$$

The product $\bar{v}_{X,s} b_{s,n}^*$ is determined by the circuit and does not depend on the variables of optimization. Note that each term of the summation is independent; the graph-based representation is condensed and orthogonalized. Consequently, power transferred by each primary can be separated and optimized independently. The expression in Equation (15) fits neatly into the paradigm of a WPT transmitter and receiver. Accounting for all the transmission paths, the power transmitted by element n to element the secondary is calculated as

$$-\bar{v}_{X,s} b_{s,n}^* \bar{v}_{X,n}^*. \tag{16}$$

Because the graph of WPT interactions has been simplified to a set of independent point-to-point WPT events, each independent transmitter–receiver pair can be optimized by maximizing each quantity described by Equation (16).

It is observed that the objective function will be maximized when the norm of the excitation is maximized, as

$$\|\bar{v}_{X,n}\| = \alpha_n \tag{17}$$

and $\bar{v}_{X,n}$ is anti-parallel to the product $\bar{v}_{X,s}b^*_{s,n}$, or

$$\bar{v}_{X,n} = \frac{-\alpha_n \bar{v}_{X,s} b^*_{s,n}}{\left\|\bar{v}_{X,s} b^*_{s,n}\right\|} \tag{18}$$

Note that the secondary excitation voltage $\bar{v}_{X,s}$ is given, and not a variable of optimization in this case. An alternative interpretation is that $V_{X,n}$ should lag $-V_{X,s}$ by the angle of $b_{s,n}$. It should be noted that in a simple reactive system with a single primary and a single secondary, the phase of the primary will either lead or lag the phase of the secondary, depending on the polarity of the primary–secondary coupling.

Recall that the phase of $\bar{v}_{X,s}$ is chosen, and other phases are measured relative to $\bar{v}_{X,s}$. Let $\bar{v}_{X,s}$ be defined as positive and real, i.e.,

$$\bar{v}_{X,s} \in \mathbb{R}_{>0}. \tag{19}$$

Typically, the impedance in a WPT system is dominated by the reactance, meaning the system is essentially lossless. In such a system,

$$\Re(b_{m,n}) = 0; \tag{20}$$

in that case, $\bar{v}_{X,n}$ should be parallel to $b_{s,n}$ for $n \neq s$, or

$$\bar{v}_{X,n} \parallel b_{s,n}. \tag{21}$$

Consider some implications of the assumptions in Equations (19)–(21):

$$\begin{aligned} \bar{v}_{X,s} \in \mathbb{R}_{>0} &\implies \bar{v}_{X,s} = \|\bar{v}_{X,s}\| \\ \Re(b_{m,n}) = 0 &\implies {b_{m,n}}^* = -b_{m,n} \\ \bar{v}_{X,n} \parallel b_{s,n} &\implies \bar{v}^*_{X,s} b_{s,n} = \|\bar{v}_{X,s}\| \|b_{s,n}\|. \end{aligned} \tag{22}$$

Substituting into Equation (15) yields

$$\begin{aligned} \Re\left(-\bar{v}_{X,s} b^*_{s,n} \bar{v}^*_{X,n}\right) &= \Re\left(-\|\bar{v}_{X,s}\| b^*_{s,n} \bar{v}^*_{X,n}\right) \\ &= \Re\left(\|\bar{v}_{X,s}\| b_{s,n} \bar{v}^*_{X,n}\right) \\ &= \Re\left(\|\bar{v}_{X,s}\| \|b_{s,n}\| \left\|\bar{v}^*_{X,n}\right\|\right), \end{aligned} \tag{23}$$

which is the maximum possible value subject to the constraints.

Note that $\bar{v}_{X,s}$ is fixed before the optimization, and is not included in the optimization. In a lossless system,

$$\Re\left(\bar{v}_{X,s} \bar{v}^*_{X,s} b^*_{s,s}\right) = 0, \tag{24}$$

and the optimization need only consider the other voltage excitations.

3.2. Comments on Invertibility

In Equation (14), it is assumed that the matrix B is invertible. The discussion on invertibility follows two tracks: in Section 3.2.1, it is shown that a realizable, solvable system implies the existence of B; in Section 3.2.2, sufficient conditions for invertibility are discussed.

3.2.1. Existence of B in a Realizable System

To prove the existence of B, the logical contrapositive will be used. Let $(Z, L, \omega) \in Y$ mean that Z, L, and ω define a realizable, solvable system. This section proves

$$\nexists B \implies (Z, L, \omega) \notin Y \tag{25}$$

to demonstrate that

$$(Z, L, \omega) \in Y \implies \exists B, \tag{26}$$

which means that B must exist in any solvable, realizable system.

In the counterexample, where $(j\omega L + Z)$ is non-invertible, it is known that $(j\omega L + Z)$ is necessarily rank-deficient:

$$\exists \mathbf{i} \neq 0 | \mathbf{v}_x = (j\omega L + Z)\mathbf{i} = 0. \tag{27}$$

That statement can be interpreted as "there exists a state where there is current through some inductors, but there is no excitation voltage", which means that current flows through the system with no excitation current. Practically, such a system is unrealizable due to parasitic resistances; any system with parasitic resistances is guaranteed to produce a viable B.

However, when the parasitic resistance is very small or unknown, it may be reasonable to model the system with ideal conductors. Even in such a system, Equation (27) implies that the effective impedance around any of the Thévenin circuits is zero. As long as the effective impedance around any loop is non-zero, the necessary matrix will be invertible.

3.2.2. Tests and Necessary Conditions for Invertibility

Future research should further develop sufficient conditions, but for now, three tests can guarantee the existence of B. If either of the following sufficient conditions are met, the system is guaranteed to be realizable with non-zero impedance, and B is guaranteed to exist.

Typically, the WPT system can be modeled as lossless, meaning that Z is imaginary. In that case, consider the reactance matrix X such that

$$Z = jX, X \in \Re. \tag{28}$$

The matrix B can be expressed as

$$B = -j(\omega L + X)^{-1}, \tag{29}$$

which is a specialized form of Equation (10) assuming purely reactive impedance. Note that L is an inductance matrix, which is necessarily positive definite, real, and symmetric. Let $\lambda_{L,1}$ be the lowest eigenvalue of ωL. Further, let $\lambda_{X,1}$ be the lowest diagonal element of X; since X is diagonal, $\lambda_{X,1}$ is the lowest eigenvalue. Let $\lambda_{B^{-1}}$ be the lowest eigenvalue of $(\omega L + X)$. The sufficient condition is that

$$\lambda_{X,1} \geq 0, \tag{30}$$

which implies

$$\lambda_{X,1} \geq 0 \implies \lambda_{L,1} + \lambda_{X,1} > 0 \implies \lambda_{B^{-1}} > 0, \tag{31}$$

therefore, none of the eigenvalues of $(\omega L + X)$ are zero, so $(\omega L + X)^{-1}$ and B must exist. The first sufficient condition is that in a lossless system, the compensating reactances are non-negative. This will occur when the Thévenin impedance is not present or generated by an inductor or a resistor; normally, however, the compensation is capacitive, requiring a different sufficient condition.

A less restrictive interpretation of Equation (31) allows negative Thévenin reactance, or capacitive compensation. If the eigenvalues of ωL are known, then a looser sufficient

condition can be derived from Equation (31). Let the Thévenin impedance be capacitive, but be bounded by the eigenvalues of ωL:

$$\lambda_{X,1} > -\lambda_{L,1}. \tag{32}$$

This leads to the conclusion

$$\lambda_{X,1} > -\lambda_{L,1} \implies \lambda_{L,1} + \lambda_{X,1} > 0 \implies \lambda_{B^{-1}} > 0 \tag{33}$$

This condition guarantees no eigenvalues of 0, proving the existence of B. The lower limit on the reactance also establishes a lower limit on the capacitor size. This allows for more realistic compensation, but can be unnecessarily restrictive when pad sizes are dissimilar: the capacitance for all pads is essentially restricted by the least inductive coil.

One approach that defines a compensation limit per pad is using Gershgorin circles, which also allows for resistive elements in the circuit. The Gershgorin circle theorem states that each eigenvalue of a matrix A must lie within a circle on the complex plane, with center points a_{ii} given as the diagonal elements of A, and radii R_i given by the sum of the absolute value of off-diagonal elements in each row. Using the Gershgorin circle theorem on the matrix $(j\omega L + Z)$ with $\lambda_{B^{-1},k}$ being an eigenvector of that matrix and z_{ii} the ith diagonal of Z yields

$$\forall \lambda_{B^{-1},k} \exists i : \left|\lambda_{B^{-1},k} - j\omega L_{i,i} - z_{ii}\right| \leq \sum_{m \neq i} |L_{i,m}|. \tag{34}$$

This states that each eigenvalue of $(j\omega L + Z)$ must be within a circle; as long as

$$\forall i, |j\omega L_{i,i} + z_{ii}| > \sum_{m \neq i} |L_{i,m}|, \tag{35}$$

none of the eigenvalues are 0 and the matrix must be invertible. The value of the compensation on each pad can be modified such that Equation (35) is always satisfied. In a poorly coupled system, the Gershgorin circle theorem is especially powerful. The three sufficient conditions described are summarized here:

- Non-negative compensation reactance, $\lambda_{X,1} \geq 0$. This essentially prohibits capacitive compensation and assumes lossless circuits, but can be applied without knowing the inductance matrix.
- Limited negative reactance, $\lambda_{X,1} \geq -\lambda_{L,1}$. This allows capacitive compensation but assumes lossless circuits and applies the same compensation restriction to all pads.
- Gershgorin circle limitation, $\forall i, |j\omega L_{i,i} + z_{ii}| > \sum_{m \neq i} |L_{i,m}|$. This allows lossy components and assigns a different compensation limit to each pad.

3.3. Extension to Multiple Secondaries

The approach in Section 3.1 can be modified to account for multiple secondary pads. Some high-power WPT applications use multiple secondary pads to maximize power transfer, or some drone applications have multiple disparate secondary coils [12]. There are many ways to define an objective function, weighting power transfer to a given coil or optimizing for total power transfer. For a DWPT application where all secondaries are connected to the same battery, the objective of optimization may be defined as the total power transferred to all secondaries. In some cases, there may be a constraint that power to any given secondary does not exceed some hardware rating, although the hardware should generally be rated high enough that such a constraint is unnecessary. For a system with n pads and k secondaries, where the secondaries are represented in the last rows of L, the optimization can be expressed as

$$\begin{aligned} \max_{\mathbf{v}_x \setminus v_{X,n}} \ & \Re\left(\sum_{l=n-k+1}^{n} -\bar{i}_l^* \bar{v}_{X,l}\right) \text{ s.t.} \\ & \bar{v}_{x,n} \text{ is given} \\ & \|\bar{v}_{X,n}\| \leq \alpha_n \ \forall n \\ & \mathbf{i} = B\mathbf{v}_X. \end{aligned} \tag{36}$$

In Equation (36), the magnitudes of all the excitation voltages are fixed, and the phase of one secondary is fixed. Although there are multiple secondaries, it is only necessary to fix the excitation voltage corresponding to one; the phase of the other secondary may vary. Two immediate consequences follow. First, the problem is no longer linear, but quadratic: there is a quadratic term in the objective function summation corresponding to each unfixed secondary excitation voltage. Second, the other secondaries have the freedom to operate at different phase angles; each of the unfixed secondaries may alter its phase to reduce reactive power or maximize power transfer to itself. The result of these two consequences is that the simple closed-form solution developed in Section 3.1 is no longer applicable, and the correlation between real/complex currents and primary/secondary excitations breaks down. However, the quadratic problem can still be easily solved by most optimizers.

A convenient closed-form solution still exists for the special case where all the secondaries are operating at fixed excitations; that is, when the secondary voltage excitations are excluded from the variables of optimization. In that case, the objective function is given by

$$\begin{aligned} \max_{\mathbf{v}_x} \ & \Re\left(\sum_{l=n-k+1}^{n} -\bar{i}_l^* \bar{v}_{X,l}\right) \text{ s.t.} \\ & \bar{v}_{x,k} \text{ is given for all } k \geq n-k+1 \\ & \|\bar{v}_{X,n}\| \leq \alpha_n \ \forall n \\ & \mathbf{i} = B\mathbf{v}_X. \end{aligned} \tag{37}$$

Note that the problem is linear when all the secondary excitations are fixed.

Similar to the calculations in Equation (15), the objective function can be expressed as

$$\begin{aligned} & \Re\left(\sum_{l=n-k+1}^{n} \left(-\bar{v}_{X,l}\bar{i}_l^*\right)\right) \\ = & -\Re\left(\sum_{l=n-k+1}^{n} \left(\bar{v}_{X,l} \sum_n b_{l,n}^* \bar{v}_{X,n}^*\right)\right) \\ = & -\sum_n \Re\left(\left(\sum_{l=n-k+1}^{n} \bar{v}_{X,l} b_{l,n}^*\right) \bar{v}_{X,n}^*\right) \end{aligned} \tag{38}$$

Similar to the single-secondary case, the objective function will be maximized when

$$\bar{v}_{x,n} = \frac{-\alpha_n \sum_{l=n-k+1}^{n} \bar{v}_{X,l} b_{l,n}^*}{\left\| \sum_{l=n-k+1}^{n} \bar{v}_{X,l} b_{l,n}^* \right\|} \tag{39}$$

3.4. A Note on Local Optimization

The graph-based structure is critical to understanding potential false assumptions about the system; such assumptions may be valid for a simple system with a single primary and a single secondary but break down in more complex systems. One such assumption is that power transfer can be maximized by individually maximizing the power transferred by each primary pad; such an assumption is briefly disproven here.

Consider a system with inductance and admittance matrices defined as

$$\begin{aligned} \omega &= 1 \\ L &= \begin{bmatrix} 1 & \frac{1}{2} & \frac{1}{3} \\ \frac{1}{2} & 1 & \frac{1}{2} \\ \frac{1}{3} & \frac{1}{2} & 1 \end{bmatrix} \\ Z &= 0, \end{aligned} \tag{40}$$

where $n = 3$ corresponds to the secondary. Note that L is positive definite, so the system is realizable. $Z = 0$ implies a system with no series compensation. Assuming $\bar{v}_{X,3} = 1$, and $\forall n, \alpha_n = 1$, the optimization yields

$$\begin{aligned} \mathbf{v}_X &= \begin{bmatrix} j & j & 1 \end{bmatrix}^T \\ \mathbf{i} &= \begin{bmatrix} -0.75 + j0.15 & -1 + j0.6 & 0.75 - j1.35 \end{bmatrix}^T \end{aligned} \tag{41}$$

with the vector of apparent power delivered by each pad

$$\mathbf{s} = \begin{bmatrix} 0.15 + j0.75 & 0.6 + j1 & -0.75 + j1.35 \end{bmatrix}^T, \tag{42}$$

so the secondary receives 0.75 W of real power.

However, consider the case where the excitations for the secondary and first primary are fixed, and then, optimize the other primary ($n = 2$) excitation to maximize real power transfer from that primary. If the primary pad only optimizes the total power it sends, regardless of whether that is to another primary or a secondary, the formulation is equivalent to the multiple-secondary approach in Equation (39). The resulting excitation currents, voltages, and apparent powers are

$$\begin{aligned} \mathbf{v}_X &= \begin{bmatrix} j & -\frac{1}{\sqrt{2}} - j\frac{1}{\sqrt{2}} & -1 \end{bmatrix}^T \\ \mathbf{i} &= \begin{bmatrix} 1.774 - j0.574 & -1.731 + j0.531 & 0.274 + j0.926 \end{bmatrix}^T \\ \mathbf{s} &= \begin{bmatrix} -0.574 + j1.774 & 0.849 + j1.6 & -0.274 + j0.926 \end{bmatrix}^T. \end{aligned} \tag{43}$$

Comparing Equation (43) with Equation (42), it can be seen that the primary $n = 2$ transfers more real power but at the expense of power transfer to the secondary. That is, optimizing power transfer locally at each primary pad is not sufficient to guarantee optimal power transfer.

4. Example

To demonstrate the effectiveness of this approach, a DWPT test simulated the graph-based optimization described here. As approximated in Equations (5)–(7), the dynamics due to the changing geometry are insignificant compared to the AC dynamics, and the DWPT system can be approximated by a series of stationary WPT systems. The power transferred during a DWPT test is indicative of the graph-based approach over a range of feasible graph configurations.

Three different systems were simulated and are visualized in Figures 2–4. All three systems are roughly in line with a DWPT system for electric vehicles. All tests have four primary pads, the first two systems have one secondary pad, and system three has two secondary pads. All the pads in all the systems are square. In all cases, the DC excitation voltage is 500 V, the air gap is 140 mm, and the vehicle assembly moves across the series of primary pads at 50 km/h. Note that the switching frequency is 85 kHz, in line with [20]. All systems are modeled in an FEM solver to determine the inductance matrix across a range of likely alignments. Those positions are as the secondary pad moves across the primary pads, with perfect alignment orthogonal to the direction of motion.

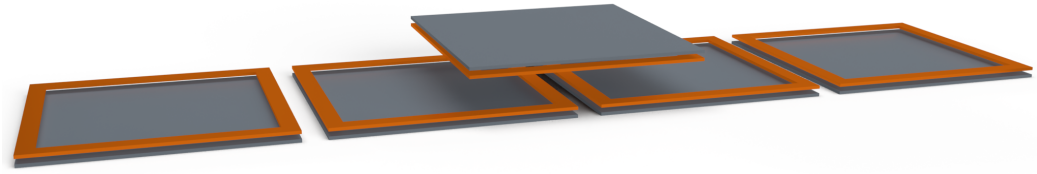


Figure 2. Illustration of example WPT system 1. Four primary (roadway) pads transfer power to a single, moving secondary (vehicle) pad.

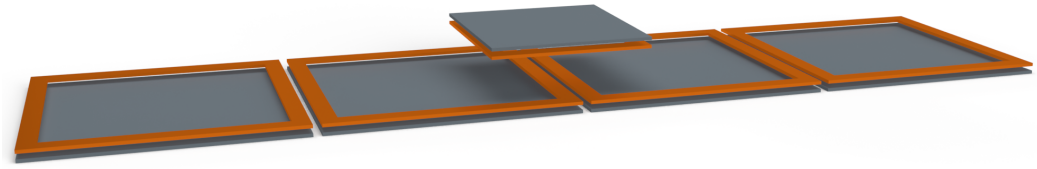


Figure 3. Illustration of example WPT system 2. Four primary (roadway) pads transfer power to a single, moving secondary (vehicle) pad. The vehicle pad is smaller than in system 1, and the pads are closer together.

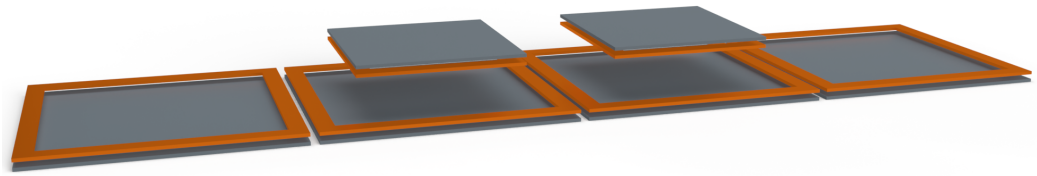


Figure 4. Illustration of example WPT system 3. Four primary (roadway) pads transfer power to two moving secondary (vehicle) pads. The pad design is the same as in system 2, but with an additional secondary pad.

Series compensation is used, with a slightly inductive load to avoid an AC short circuit and ensure the potential for zero-volt switching; the compensation impedance is a 350 nF capacitor in all cases. The inductance is boosted by including a ferrite plate outside each coil of the same dimensions as the coil. The gap between the coil and ferrite is 15 mm and the thickness of both the ferrite and the coil is 10 mm. The circuit diagram for each pad in all systems is given in Figure 5, and values are shown in Table 1.

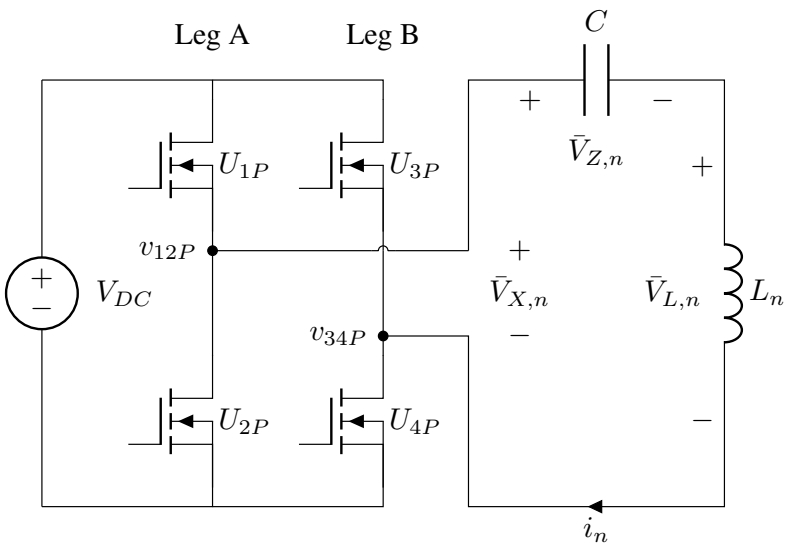


Figure 5. Circuit diagram; note that the primary and secondary pads are all identical.

Table 1. Typical WPT parameters for each geometry.

System Number	Primary Pad Dimension	Secondary Pad Dimension	Pad Spacing	Primary Turns	Secondary Turns
1	750 mm	750 mm	850 mm	3	3
2	750 mm	500 mm	775 mm	3	4
3	750 mm	500 mm	775 mm	3	4

Three different control schemes are compared here. The first control scheme is the naive approach, where each pad operates at a set phase and the primary pads lead the secondary pads by 90°. The second control scheme is the inductor-based approach, where the phase of each primary excitation corresponds to the sign of the primary–secondary coupling at that point. In the absence of other primary pads, this approach would be optimal. Note that the inductor-based control scheme is ambiguous in the multi-secondary system; here, the sign of the sum of both primary–secondary couplings for a single primary is used. The third control scheme is the optimal approach described in detail in this paper, which accounts for power flow through the network. For systems 1 and 2, the closed-form solution in Equation (18) is used; for the multi-secondary system 3, the quadratic optimization in Equation (36) is used.

The plots of power with all three approaches are shown in Figures 6–8, with the total power transferred given in Table 2. From Table 2, it can be seen that the graph-based method outperforms the other methods. This performance boost is achieved without increasing the excitation voltages, but simply by exploiting the parasitic coupling. This exemplifies the thesis of this paper; that the graph-based approach allows an engineer to push maximum power to the secondary pad and that such an approach is guaranteed to outperform other control strategies.

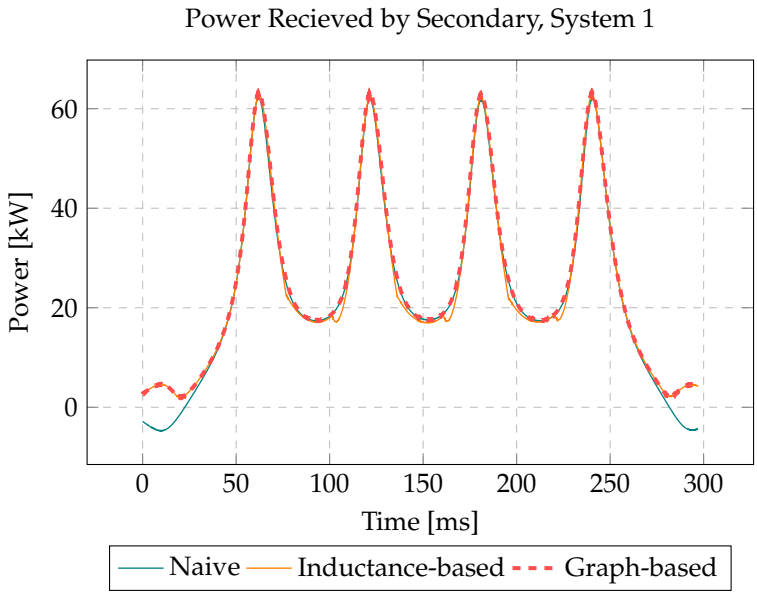


Figure 6. Comparison of three approaches. Power is smoothed by a low-pass filter with a corner frequency of 42.5 Hz. Note that the inductance-based method underperforms on the troughs, and the basic method underperforms at the beginning and the end.

In Figure 6, observe that the inductance-based approach underperforms compared to the other approaches; at those brief moments, the naive approach happens to correspond with the optimal approach. Similarly, at the beginning and the end, the naive approach causes a primary pad to pull power from the negatively coupled secondary pad, while the inductor-based approach coincides with the graph-based, optimal approach. In those regions, the naive approach underperforms compared to the other two approaches. Only the

graph-based approach accounts for both phenomena. However, the difference between the approaches is relatively small, with only a 6.3 % improvement over the worst-case scenario.

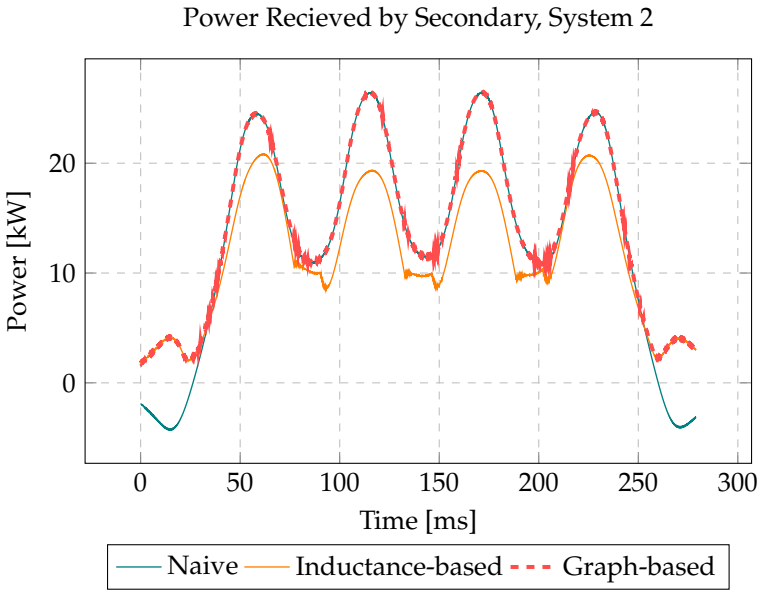


Figure 7. Comparison of three approaches. Power is smoothed by a low-pass filter with a corner frequency of 42.5 Hz. Note that the inductance-based method underperforms on the troughs, and the basic method underperforms at the beginning and the end.

In Figure 7, the inductance-based approach performs worse across nearly the entire range. In a system with only one primary pad and one secondary, the inductance-based approach is optimal. However, with the graph structure derived from the geometry depicted in Figure 3, the parasitic couplings play a greater role. The graph-based approach and the naive approach coincide over most possible graph structures. However, at the extrema, when the secondary is only coupled strongly to one primary pad, the inductor-based and graph-based models suggest the same strategy. As in the first system, the graph-based model can be optimized to transmit more power than either alternative.

Table 2. Energy transferred to secondary pad(s) for each system and control algorithm. The "relative improvement" field relates the total energy transferred to the lowest-energy variant of the same system.

System Number	Control Scheme	Energy Transferred	Relative Improvement
System 1	Naive	7.00 kJ	N/A
System 1	Inductance-based	7.24 kJ	3.5 %
System 1	Graph-based	7.44 kJ	6.3 %
System 2	Naive	3.71 kJ	12.7 %
System 2	Inductance-based	3.30 kJ	N/A
System 2	Graph-based	4.04 kJ	22.3 %
System 3	Naive	7.49 kJ	4.3 %
System 3	Inductance-based	7.18 kJ	N/A
System 3	Graph-based	8.27 kJ	15.2 %

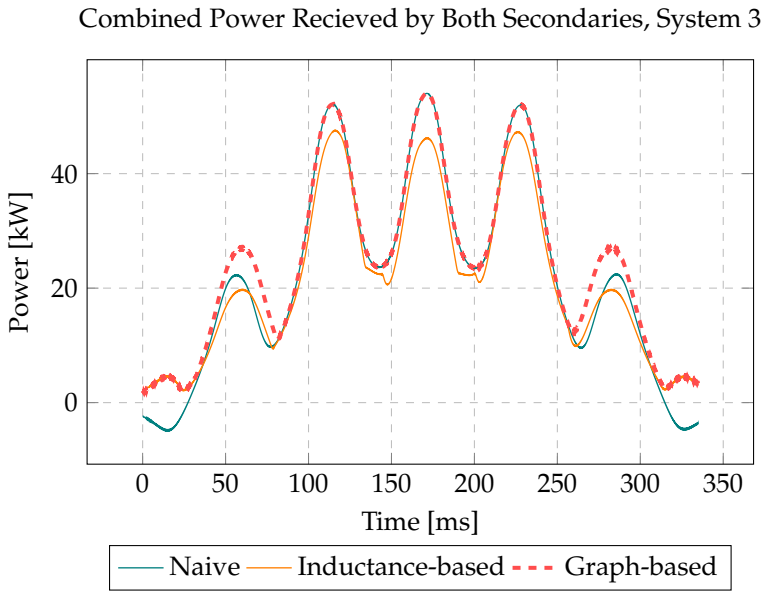


Figure 8. Comparison of three approaches. Power is smoothed by a low-pass filter with a corner frequency of 42.5 Hz. Note that the inductance-based method underperforms on the troughs, and the basic method underperforms at the beginning and the end.

There are five peaks in Figure 8; the addition of another secondary pad introduces another position where power can be transferred. As in the other cases, power transfer is improved with the graph-based model relative to the two baseline algorithms. Recall that in all cases the magnitudes of the excitation voltages are constant. By accounting for all possible transmission paths in the system, the graph-based approach allows greater energy to be transferred with the same excitation voltages.

As noted in [14], a lower total impedance (including the coil and the compensation) allows higher power transfer levels. Each coil, acting as a primary, has a lower impedance between the excitation voltage and the induced voltage, forcing more current through the circuit. Similarly, each coil, acting as a booster coil, amplifies the current with a lower impedance, which amplifies the booster-coil properties. Any change to the system that boosts primary–primary coupling or lowers impedance will transfer more power, disproportionately affecting the graph-based approach presented here.

Systems that emphasize one primary–secondary link above others, such as with a smaller secondary coil, also highlight the power of the approach described in this work. In that case, the single strong primary–secondary link concentrates the impact of all the primary voltage excitations through a single edge, which is more powerfully modeled by this approach.

5. Conclusions

The approach presented here allows the complex interactions of mutually coupled WPT pads to be modeled with a graph. This allows pads to simultaneously act as primaries, secondaries, and booster coils. The parasitic primary–primary coupling can be exploited to force each primary pad to behave like a booster coil, acting as a via and a source.

Stability conditions for compensation are discussed, with two definitions of maximum compensating inductance established. Increasing the compensating impedance helps transfer power, but if the compensating impedance increases beyond some threshold, the power transfer may become unstable.

An omniscient, optimal controller is developed. Exploiting that model allows the primary pads to switch smartly, increasing the total power transfer by up to 25% compared to a baseline approach, as verified in Section 4. In all the test cases, the magnitude of the voltage excitations did not vary; increases in total power transfer with the graph-based approach were achieved by accounting for all transmission paths from a primary pad

to all secondary pads. The results indicate that the proposed control scheme is effective regardless of circuit topology. Considerations are included for a multi-secondary system. The resulting system is stable and more effective than either of the other two approaches considered, as demonstrated in a simulation.

A hardware-based experimental validation of the innovations discussed herein is deferred for future work. Hardware experimentation would validate the FEM results, but that is beyond the scope of this work. Further, a practical hardware system would require an omniscient controller, the development of which is best suited for a follow-up manuscript.

The approach is developed within an EV charging paradigm but promises utility in other applications, as well. Charging a swarm of drones, for example, could use the approach developed here. Modeling or optimizing the placement of booster coils could also use the tools developed here. Within DWPT and other potential applications, this work opens new avenues of research; the two most prominent of which are, first, evaluating the controllability and stability of a graph-based WPT system, and second, measuring or controlling transient response. While both discussions are beyond the scope of the present work, the present work lays the foundation for future work, which will enrich the present contributions.

Author Contributions: Conceptualization, M.J.H.; methodology, M.J.H. and G.D.; software, M.J.H.; validation, M.J.H., G.D. and A.K.; formal analysis, G.D.; investigation, M.J.H.; writing—original draft preparation, M.J.H.; writing—review and editing, G.D. and A.K.; visualization, M.J.H.; supervision, G.D. and A.K.; project administration, G.D.; funding acquisition, A.K. All authors have read and agreed to the published version of the manuscript.

Funding: This research was supported in part by the ASPIRE (Advancing Sustainability through Powered Infrastructure for Roadway Electrification) Center, an NSF ERC, under award number 1941524. The APC was waived.

Data Availability Statement: The raw data supporting the conclusions of this article will be made available by the authors on request.

Conflicts of Interest: The authors declare no conflicts of interest.

References

1. Limb, B.J.; Asher, Z.D.; Bradley, T.H.; Sproul, E.; Trinko, D.A.; Crabb, B.; Zane, R.; Quinn, J.C. Economic Viability and Environmental Impact of In-Motion Wireless Power Transfer. *IEEE Trans. Transp. Electrif.* **2019**, *5*, 135–146. [CrossRef]
2. Dai, J.; Ludois, D.C. A Survey of Wireless Power Transfer and a Critical Comparison of Inductive and Capacitive Coupling for Small Gap Applications. *IEEE Trans. Power Electron.* **2015**, *30*, 6017–6029. [CrossRef]
3. Ahmad, A.; Alam, M.S.; Mohamed, A.A.S. Design and Interoperability Analysis of Quadruple Pad Structure for Electric Vehicle Wireless Charging Application. *IEEE Trans. Transp. Electrif.* **2019**, *5*, 934–945. [CrossRef]
4. Pries, J.; Galigekere, V.P.N.; Onar, O.C.; Su, G.J. A 50-kW Three-Phase Wireless Power Transfer System Using Bipolar Windings and Series Resonant Networks for Rotating Magnetic Fields. *IEEE Trans. Power Electron.* **2020**, *35*, 4500–4517. [CrossRef]
5. Hariri, A.O.; Youssef, T.; Elsayed, A.; Mohammed, O. A Computational Approach for a Wireless Power Transfer Link Design Optimization Considering Electromagnetic Compatibility. *IEEE Trans. Magn.* **2016**, *52*, 7205704. [CrossRef]
6. Buja, G.; Bertoluzzo, M.; Mude, K.N. Design and Experimentation of WPT Charger for Electric City Car. *IEEE Trans. Ind. Electron.* **2015**, *62*, 7436–7447. [CrossRef]
7. Hansen, M.; Poddar, S.; Ahmed, H.; Kim, S.; Kamineni, A. Artificial Neural Network Modeling of WPT Magnetic Fields in an EV Application. In Proceedings of the 2023 IEEE Wireless Power Technology Conference and Expo (WPTCE), San Diego, CA, USA, 4–8 June 2023; pp. 1–6. [CrossRef]
8. Shen, S.; Zhang, Z.; Wu, Y.; Wang, R.; Liang, Z. Modeless Prediction of Variable Coupling Effect for Multiple-Load Wireless Power Transfer. *IEEE Trans. Magn.* **2022**, *58*, 1–5. [CrossRef]
9. Hansen, M.; Kamineni, A.; Zane, R. Zero-Crossing Current Detection for Modular and Robust Dynamic Wireless Power Transfer. In Proceedings of the 2020 IEEE Energy Conversion Congress and Exposition (ECCE), Detroit, MI, USA, 11–15 October 2020; pp. 5207–5214. [CrossRef]
10. Azad, A.N.; Echols, A.; Kulyukin, V.A.; Zane, R.; Pantic, Z. Analysis, Optimization, and Demonstration of a Vehicular Detection System Intended for Dynamic Wireless Charging Applications. *IEEE Trans. Transp. Electrif.* **2019**, *5*, 147–161. [CrossRef]
11. Kamineni, A.; Neath, M.J.; Zaheer, A.; Covic, G.A.; Boys, J.T. Interoperable EV Detection for Dynamic Wireless Charging with Existing Hardware and Free Resonance. *IEEE Trans. Transp. Electrif.* **2017**, *3*, 370–379. [CrossRef]

12. Zhang, Z.; Shen, S.; Liang, Z.; Eder, S.H.K.; Kennel, R. Dynamic-Balancing Robust Current Control for Wireless Drone-in-Flight Charging. *IEEE Trans. Power Electron.* **2022**, *37*, 3626–3635. [CrossRef]
13. Sarin, A.; Avestruz, A.T. A Framework for Code Division Multiple Access Wireless Power Transfer. *IEEE Access* **2021**, *9*, 135079–135101. [CrossRef]
14. Ota, Y.; Takura, T.; Sato, F.; Matsuki, H. Wireless power transfer by low coupling electromagnetic induction—LC booster. In Proceedings of the 2012 IEEE MTT-S International Microwave Workshop Series on Innovative Wireless Power Transmission: Technologies, Systems, and Applications, Kyoto, Japan, 10–11 May 2012; pp. 175–178. [CrossRef]
15. Liu, W.; Chau, K.T.; Lee, C.H.T.; Jiang, C.; Han, W.; Lam, W.H. Multi-Frequency Multi-Power One-to-Many Wireless Power Transfer System. *IEEE Trans. Magn.* **2019**, *55*, 1–9. [CrossRef]
16. Oh, H.; Oh, S.; Koo, H.; Choi, W.; Shin, J.; Hwang, K.C.; Lee, K.Y.; Yang, Y. Mid-Range Wireless Power Transfer System for Various Types of Multiple Receivers Using Power Customized Resonator. *IEEE Access* **2021**, *9*, 45230–45241. [CrossRef]
17. Bai, T.; Mei, B.; Zhao, L.; Wang, X. Machine Learning-Assisted Wireless Power Transfer Based on Magnetic Resonance. *IEEE Access* **2019**, *7*, 109454–109459. [CrossRef]
18. Ahn, D.; Hong, S. Effect of Coupling between Multiple Transmitters or Multiple Receivers on Wireless Power Transfer. *IEEE Trans. Ind. Electron.* **2013**, *60*, 2602–2613. [CrossRef]
19. Bono, J.; Ahmed, H.; Nimri, R.; Kamineni, A. Current Distribution in Multifilar Wireless Charging Pads. In Proceedings of the 2023 IEEE Wireless Power Technology Conference and Expo (WPTCE), San Diego, CA, USA, 4–8 June 2023.
20. *SAE Standard J2954_202208*; Wireless Power Transfer for Light-Duty Plug-in/Electric Vehicles and Alignment Methodology. SAE: Warrendale, PA, USA, 2022. [CrossRef]
21. Pantic, Z.; Bai, S.; Lukic, S.M. ZCS *LCC*-Compensated Resonant Inverter for Inductive-Power-Transfer Application. *IEEE Trans. Ind. Electron.* **2011**, *58*, 3500–3510. [CrossRef]

Disclaimer/Publisher's Note: The statements, opinions and data contained in all publications are solely those of the individual author(s) and contributor(s) and not of MDPI and/or the editor(s). MDPI and/or the editor(s) disclaim responsibility for any injury to people or property resulting from any ideas, methods, instructions or products referred to in the content.